Version: Published Version

eprints@whiterose.ac.uk
https://eprints.whiterose.ac.uk/

The structure and mechanics of the cell cortex depend on the location and adhesion state

D. A. D. Flormann[a], L. Kainka[a], G. Montalvo[a] (ID), C. Anton[a], J. Rheinlaender[b], D. Thalla[a], D. Vesperini[a] (ID), M. O. Pohland[a], K. H. Kaub[a,c], M. Schu[a], F. Pezzano[d] (ID), V. Ruprecht[d,e,f] (ID), E. Terriac[a] (ID), R. J. Hawkins[g,h], and F. Lautenschläger[a,i,1] (ID)

Affiliations are included on p. 8.

Cells exist in different phenotypes and can transition between them. A phenotype may be characterized by many different aspects. Here, we focus on the example of whether the cell is adhered or suspended and choose particular parameters related to the structure and mechanics of the actin cortex. The cortex is essential to cell mechanics, morphology, and function, such as for adhesion, migration, and division of animal cells. To predict and control cellular functions and prevent malfunctioning, it is necessary to understand the actin cortex. The structure of the cortex governs cell mechanics; however, the relationship between the architecture and mechanics of the cortex is not yet well enough understood to be able to predict one from the other. Therefore, we quantitatively measured structural and mechanical cortex parameters, including cortical thickness, cortex mesh size, actin bundling, and cortex stiffness. These measurements required developing a combination of measurement techniques in scanning electron, expansion, confocal, and atomic force microscopy. We found that the structure and mechanics of the cortex of cells in interphase are different depending on whether the cell is suspended or adhered. We deduced general correlations between structural and mechanical properties and show how these findings can be explained within the framework of semiflexible polymer network theory. We tested the model predictions by perturbing the properties of the actin within the cortex using compounds. Our work provides an important step toward predictions of cell mechanics from cortical structures and suggests how cortex remodeling between different phenotypes impacts the mechanical properties of cells.

actin | cortex | cytoskeleton | cells | suspended

Actin is the most abundant protein in eukaryotic cells (1). Its filamentous form, in combination with microtubules and intermediate filaments, defines the cytoskeleton (2). The main structure responsible for the mechanical properties of cells is the actin cortex, which is a filamentous network of actin assembled directly under the plasma membrane (3). Interacting with the actin filaments are many actin-binding proteins such as nucleators, cross-linkers, bundling proteins, and molecular motors (4–8). As the actin cortex is such a pivotal cellular element, it has stimulated a lot of studies, especially for its roles in cell mitosis, migration, and differentiation (1, 3, 9–11). Key to the function of these cell processes are the structure and mechanics of the cortex (12, 13). However, the mechanisms of how the structure is related to the mechanics of the cell cortex are not yet well understood.

Simpler actin networks studied in vitro have led to some helpful insights into the relationship between structure and mechanics which might be relevant in living cells. Gardel et al. (14) investigated in vitro the effect of the concentration of actin and cross-linkers on network stiffness using a parallel plate bulk rheometer. In their work, a constant cross-linker concentration with an increasing actin concentration resulted in a decrease of actin mesh size and a subsequent increase of stiffness, showing a negative correlation between the actin mesh size and its stiffness. This is consistent with earlier theoretical work by MacKintosh et al. (15). However, when Gardel et al. (14) kept the actin concentration constant and increased the cross-linker concentration, the mesh size also increased but resulted in an increase of stiffness due to thicker actin bundles. So, in this case, the actin mesh size and the stiffness were positively correlated. This positive correlation is also consistent with the theory in ref. 15 assuming cross-linking increases bundling.

Due to its importance in biology (16, 17), we wondered how the actin mesh size correlates with stiffness in living cells. Because of the large number of actin-binding proteins present in living cells (4, 18), the regulation of the actin cortex is considerably more complex than that of minimalistic in vitro reconstituted networks. Regulation of the actin cortex can lead

Significance

The actomyosin cortex plays a dominant role in determining cell mechanics and therefore a plethora of cellular functions such as migration, division, and differentiation. Understanding the relationship between the structure and mechanics of the cortex in different situations is necessary to explain cell properties crucial to health and disease, for example, cancer. Therefore, we quantitatively characterized the cortex in suspended and adhered cells and found significant differences. We show a clear correlation between the structure and stiffness of the cortex. Aspects of our data in cells fit with earlier theoretical predictions based on in vitro experiments. We provide an important step toward predicting and controlling the mechanical behavior and therefore function of cells from the underlying structure of their cortex.

to changes in its properties when cells are in different situations (19). For example, consider a white blood cell suspended in the blood flow. To respond to immune system signaling it adheres to the blood vessel walls prior to transmigration (20). Since the behavior of adhered and suspended cells differs (21), we questioned whether the properties of their cortices differ. Therefore, we investigated the amount and structure of actin and myosin as well as the cortex stiffness in adhered and suspended cells (Fig. 1*A*) by fluorescence microscopy. To test our understanding of the relationships between structure and mechanics, we used commercial compounds to alter the concentrations of actin and myosin in the system.

We used a combination of fluorescence and scanning electron microscopy (SEM) (22) to measure the structure of the cortex of Human telomerase reverse transcriptase-immortalized retinal

pigment epithelial cells (hTERT-RPE1 cells). In particular, we measured the cortical mesh size, thickness of the actin cortex and amount of actin and myosin in both adhered and suspended cells. To investigate the mechanical properties we used atomic force microscopy (AFM) (23) (Fig. 1*B*). In the case of adhered cells, we considered two distinct regions: the nuclear and the perinuclear region (Fig. 1*C*). The full description of the methods and analysis can be found in *SI Appendix, Materials and Methods*.

Results and Discussion

We expect changes in mesh size and stiffness with changes in actin concentrations. Initial measurements of the amount of actin in the cortex of adhered and suspended cells using fluorescent
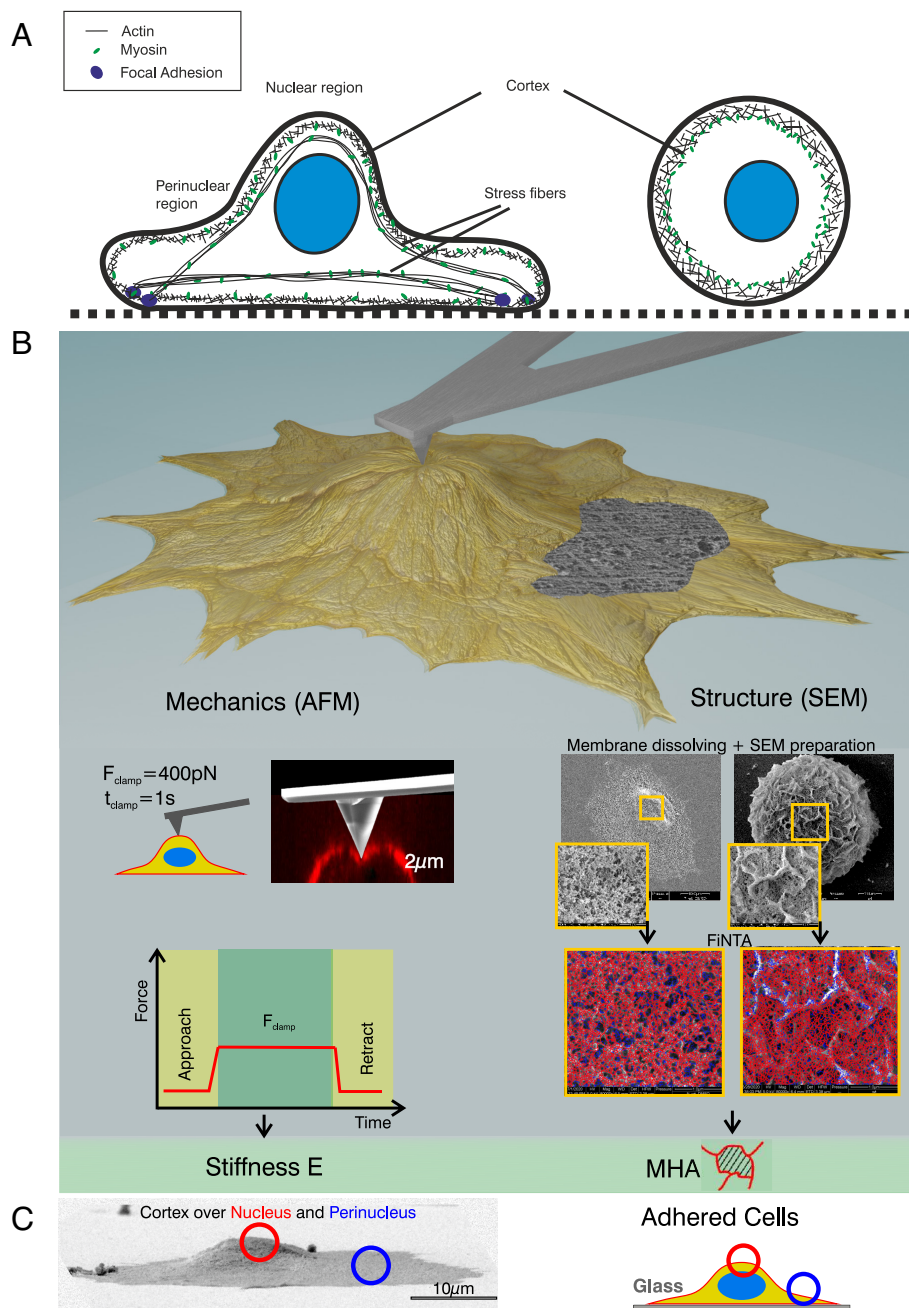
Fig. 1. Overview of adhesion states and investigation methods. (*A*) Scheme of the actin–myosin cortex of an adhered versus a suspended cell. (*B*) Overview of methods used: Mechanics was measured by atomic force microscopy (AFM), the cortex structure by scanning electron microscopy (SEM) followed by a mesh analysis using a filament network-tracing algorithm (FiNTA). (*C*) The cortex of adhered cells was analyzed at two different locations: one location directly above the nucleus (nucleus) and one in the periphery of the nucleus (perinucleus).

microscopy showed different amounts of F-actin per unit area (*SI Appendix,* Fig. SI1). This convinced us that cells in different adhesive states provide a test bed for our investigation of the mesh size and stiffness of the cortex.

The Structure of the Actin Network Depends on the Cell Location and Adhesion State. Cell mechanics is dependent on the structure of the actin network. We characterized the structure of the actin cortex by measuring three key parameters namely the cortex thickness, filament bundling, and the mesh size.

Actin cortex thickness differs depending on the cell location and adhesion state. To deepen our investigation of the amount of actin in different cell locations, we measured the thickness of the actin cortex. Previously, this has only been done before in suspended cells where the measurement can be made in the horizontal plane (24, 25). For adhered cells, the thickness measurement is difficult due to the limited resolution in z (26). To avoid this problem and increase the resolution to a maximum, we did measurements on the apical side of the cell using expansion microscopy (27) on a cross-section of adhered cells to obtain the thickness in the highest resolution available in the xy plane (Fig. 2 *A* and *B* and *SI Appendix,* Fig. SI2), thus allowing us to measure the thickness of the cortex in adhered cells (Fig. 2 *C* and *D*).

We found that in adhered cells, the nuclear and perinuclear regions of the cortex have a similar cortex thickness (Fig. 2*E*). However, in suspended cells, the cortex is thicker (Fig. 2*E*) than in adhered cells. The values we find are similar to those found by Clark et al. (28).

Actin bundling differs depending on the cell location and adhesion state. Gardel et al. showed that actin bundling has an important effect on network mechanics in vitro (14, 29). To test whether bundling is important in the actin cortex of living cells, we investigated differences in bundles of actin in our different regions of interest.

We analyzed our SEM images by tracing the network connections of particular thicknesses using our own and commercial software [e.g., filament network-tracing algorithm (FiNTA) (30) (*SI Appendix,* Fig. SI4), Filament Sensor2.0 (31), and Fiji (32)]. However, none of these tools were able to quantify the bundling in the actin cortex, e.g., FiNTA double counts some thick filament bundles as two single filaments and is generally ill-suited to capturing bundling (*SI Appendix, Actin Bundles Analysis Using FiNTA* and Fig. SI4). We therefore estimated the number of bundles by hand (Fig. 2 *F* and *G* and *SI Appendix,* Fig. SI5) classifying each image into one of three categories; no, few (1-5), or many (>5) bundles. From this, we conclude that suspended cells contain very few bundles, most bundles are in the perinuclear region of adhered cells and some in the nuclear region.

Many different actin-binding proteins may be responsible for bundling (6). If such a protein were differently expressed in adhered and suspended cells, it could explain the differences in bundling we observe. One such candidate is myosin (33). We found that the distribution of myosin as quantified from fluorescent images is different in suspended and adhered cells. However, myosin cannot be responsible for the bundling we see since there is more myosin in suspended cells where we see less bundling (*SI Appendix, Myosin II*).

There are also physical explanations for bundle formation based on depletion forces, electrostatic interactions (34–36), and mechanical strain. When cells are placed under strain, they may form focal adhesions that are connected by stress fibers (37). It is also known that strain can induce the alignment of filaments in polymer networks such as actin (38, 39). Such alignment may cause what we see as bundles in our SEM images and cause strain stiffening (40, 41) in a similar way as the bundles formed by

cross-linkers in Gardel et al.'s work (14). We note that a strain alignment mechanism for bundling could fit with our observation of more bundles in the perinuclear region compared to the nuclear region. This might indicate that the perinuclear region experiences more mechanical strain compared to the nuclear region.

Mesh Size and Stiffness of the Actin Cortex Positively Correlate. The third key characteristic of the actin cortex is the network mesh size. We recently developed a robust method to visualize (22) and quantitatively analyze (30) the cortical mesh size from SEM images (Fig. 3*A*). Interestingly, the mean mesh hole area (MHA) of the cortex differed significantly between suspended cells and the nuclear and perinuclear regions of adhered cells (Fig. 3*A*).

We expect the mesh size to affect the stiffness of the cortex. To determine the stiffness, we used AFM to deform the surface and measured the force-distance curves (23). We found significant differences in stiffness between the cortex of suspended cells and the nuclear, perinuclear regions of adhered cells (Fig. 3*B*). We further confirmed these trends with AFM measurements in HeLa cells (*SI Appendix,* Fig. SI8*C*).

Next, we investigated the correlation between the MHA and stiffness. We find a clear positive correlation between stiffness and mesh size (Fig. 3*C*). We found that fluidity is inversely correlated with mesh size (42), which is consistent with the general observation that stiffness and fluidity are inversely correlated in living cells (43, 44). Fluidity measurement data are shown in *SI Appendix,* Fig. SI6*A*. To ensure that our AFM method using a sharp pyramidal tip does not lead to distortions, we took some measurements with a colloidal tip for comparison and found that the trends are similar, i.e., the perinuclear region is stiffer than the nuclear region (*SI Appendix,* Fig. SI6*B*). We used the sharp pyramidal tip in all future measurements since it is easier to obtain localized data on the perinuclear region than with a colloidal tip. Additionally, we used AFM to image a stiffness map of whole cells (*SI Appendix,* Fig. SI7). These maps do not show any obvious stress fibers. We therefore conclude that the indentation we are using is small enough (400 nm on average, *SI Appendix,* Fig. SI8) that we are measuring the actin cortex but not any underlying actin stress fibers.

We next describe the differences we observed between nuclear and perinuclear regions of adhered cells and between these and suspended cells. We explain these differences using densely cross-linked semiflexible biopolymer theory.

Mesh size and stiffness increase in the perinuclear compared to nuclear region of adhered cells. We find that both the mesh size and stiffness are larger in the perinuclear region compared to the nuclear region (Fig. 3 *A* and *B*), i.e., there is a positive correlation between mesh size and stiffness. It is striking to note that this positive correlation agrees with the densely cross-linked semiflexible biopolymer theory (15), in which the elastic modulus (stiffness) is given by

$$G \sim \frac{K_B{}^2}{k_B T \xi^5}, \qquad [\mathbf{1}]$$

where the thermal energy is $k_B T$, and the bending rigidity of an actin bundle is $K_B \sim D_B{}^4$ where D_B is the bundle thickness. Gardel et al. (14) and Shin et al. (29) found in their in vitro experiments that the bundle thickness depends on the cross-linker to actin ratio as $D_B \sim ([crosslink]/[actin])^{0.3}$. The mesh size, ξ, is related to the bundle thickness and the concentration of actin, $\xi \sim D_B/[actin]^{1/2}$ and therefore
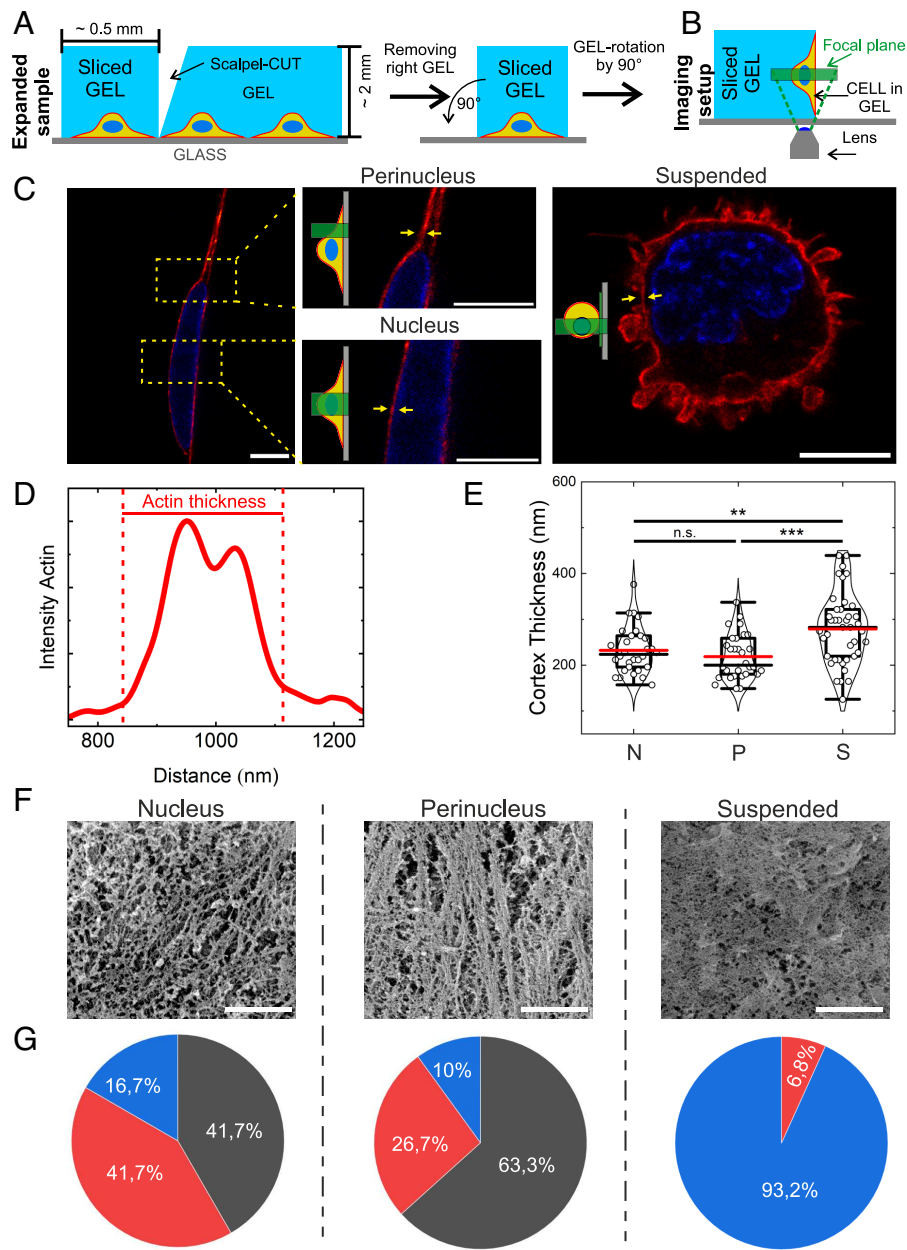
Fig. 2. In suspended cells, the actin cortex is thicker than in adhered cells but contains fewer bundles. (*A*) Scheme of the preparation procedure for side-view imaging of adhered cells using expanded samples. (*B*) Final imaging setup after gel (and hence cells) was rotated by 90° to enable side-view imaging. This is further illustrated in *SI Appendix*, Fig. SI2. (*C*) Side view of expanded nuclear and perinuclear regions as well as suspended hTERT-RPE1 cells imaged with expansion microscopy in combination with confocal imaging (Airyscan 2). Yellow arrows indicate representative measurement areas. The protocol for choosing the regions for measurements is provided in *SI Appendix*, Fig. SI3. All scale bars: 10 μm. (*D* and *E*) Analysis of intensity profiles leads to actin cortex thickness. The red horizontal lines represent the means of the distributions, and the black horizontal lines represent the medians of the distributions. In the graph (*E*), each dot represents a region. (*F*) Representative example SEM images of the cortex in the nuclear and perinuclear regions of adhered cells and the cortex of suspended cells (*Left* to *Right*) (Scale bar: 1 μm.) (*G*) Pie charts of the percentage of images showing many (black, over 5 bundles per region of interest (ROI)), few (red, between 1 and 5 bundles per ROI), or no (blue, no bundles per ROI) bundles in images like the example ones in *F* (~30 images per region). The star method is representing statistical Welch-corrected *t* tests: n.s.: not significant, *$P < 0.05$, **$P < 0.01$, ***$P < 0.001$. Cell counts: n = 10. Numbers of total measurements: ventral: nucleus = 30 (3 per cell), perinucleus = 30 (3 per cell), suspended cells = 41 (at least three per cell).

$$G \sim \frac{[actin]^{5/2} D_B{}^3}{k_B T}. \qquad [2]$$

The concentration of actin, [*actin*], in the cortex depends not only on the thickness but also on the mesh size, which we analyzed (Fig. 3). The total length of filamentous actin in the cortex is proportional to the thickness, *h*, divided by the MHA ξ^2. From our measurements, we calculate hξ^{-2} to be 0.07 nm^{-1} in the nuclear region, 0.06 nm^{-1} in the perinuclear region, and 0.10 nm^{-1} in suspended cells. From this, we conclude that the amount

of F-actin in the nuclear and perinuclear cortex regions of adhered cells is similar but that the amount of actin in the cortex of suspended cells is larger.

For constant actin concentration in adhered cells therefore

$$G \sim D_B{}^3 \sim \xi^3, \qquad [3]$$

i.e., a positive correlation between stiffness and mesh size is expected. This theory assumes that a larger mesh size with no change in the amount of actin is due to increased cross-linking causing thicker actin bundles between larger holes. Since thicker bundles are

Fig. 3. Structure and mechanics of the cellular cortex of adhered (nucleus and perinucleus) and suspended hTERT-RPE1 cells. (*A*) The MHA of the actin cortex was quantitatively analyzed using SEM images and the analysis software FiNTA. (*B*) The stiffness was quantitatively analyzed employing creep compliance measurements using AFM. (*C*) Correlation plots between MHA and stiffness (Pearson R = 0.96). Stars represent statistical difference as quantified with Welch-corrected *t* tests. Green stars compare controls to nucleus controls, and purple stars compare suspended controls to perinucleus controls. n.s.: not significant, *P < 0.05, **P < 0.01, ***P < 0.001. Cell numbers n are in the order Structure (SEM): nucleus: n = 63; perinucleus: n = 57; suspended cells: n = 66; Mechanics (AFM): nucleus: n = 53; perinucleus: n = 52; suspended cells: n = 42. The dots in Fig. 3*A* represent individual region (field of view) captured for analysis, and the dots in Fig. 3*B* represent individual cell. The control measurements in Figs. 3 and 4 are the same. For the AFM measurements on suspended cells, we excluded cells that were rolling during the measurements.

stiffer, this explains the higher stiffness. For their in vitro system, Gardel et al. (14) and Shin et al. (29) analyzed EM images and show that $D_B \sim ([crosslink]/[actin])^{0.3}$ and therefore

$$\xi \sim \frac{[crosslink]^{0.3}}{[actin]^{0.8}}. \qquad [4]$$

In Eq. **4**, the larger mesh size is due to a larger amount of cross-linking and therefore bundling.

In section actin cortex thickness, we observe that the amount of actin in adhered cells is similar in the nuclear and perinuclear regions, and we would therefore expect Eq. **3** to hold. Our results agree with Eq. **3** in that we see a positive correlation between stiffness and mesh size in the different regions of adhered cells (Fig. 3). In our SEM images, we also see more bundling in the perinuclear region compared to the nuclear region (Fig. 2*G*) indicating that the increased mesh size and increased stiffness are indeed due to actin bundles, as in Eq. **3**. Therefore, we expect that there may be an increase in cross-linking in the perinuclear region compared to the nuclear region as in Eqs. **3** and **4**.

Mesh size and stiffness decrease in suspended compared to adhered cells. Suspended cells also show a positive correlation between mesh size and stiffness but both are lower than in adhered cells (Fig. 3). This is consistent with our understanding that an increase in F-actin concentration leads to a smaller mesh size (14). In suspended cells, we see almost no bundling (Fig. 2) but we see a denser actin network with a smaller mesh size (Fig. 3). The decrease in stiffness we measure is consistent with a decrease in bundling, despite the increase in the amount of actin.

Effects of Chemical Treatment on Mesh Size and Stiffness. We found differences between the mesh size and stiffness in suspended cells compared to adhered cells (Fig. 3). These differences are consistent with the changes in actin concentration and bundling that we observe, as discussed in the previous sections. To further test our understanding of the system we used blebbistatin, an inhibitor of myosin II activity (45), and latrunculin A, an inhibitor of actin polymerization (46) to manipulate actin and myosin II in the cells (Fig. 4). We used drug concentrations small enough to not destroy the actin cortex (*SI Appendix*, Fig. SI9). Specifically, we measured the mesh size (Fig. 4*A*), stiffness (Fig. 4*B*), and bundling (Fig. 4*C*). In Fig. 4, we compare control cells (the same data as presented in Fig. 3) to blebbistatin- and latrunculin A–treated cells.

Blebbistatin does not alter the bundling of actin. The distribution of myosin II (*SI Appendix*, Fig. SI10) as well as a detailed discussion of the effects of myosin II on the mesh size (Fig. 4*A*) and stiffness (Fig. 4*B*) of cells can be found in *SI Appendix*. Inhibiting myosin II activity using blebbistatin did not, as we had expected, alter the bundling of actin (Fig. 4*C* and *SI Appendix, Myosin II Is Not Bundling Actin*) and was therefore not included in our theoretical description (*Discussion and Conclusion*).

Stiffness decreases and mesh size increases with latrunculin a treatment. Latrunculin A inhibits polymerization of actin (46). As demonstrated by Laplaud et al. (25) and Cartagena-Rivera et al. (47), actin treated with latrunculin A continues its depolymerization process without subsequent repolymerization, leading to a decrease in the overall concentration of polymerized actin filaments, which leads to a thinner actin cortex (25).

In adhered cells, we observed that the mesh size increases after latrunculin A treatment (Fig. 4*A*). This is what we expect due to the decreased concentration of actin, as shown in Eq. **4**. Physically, we expect latrunculin A to decrease the amount of actin sufficiently to break thin bundles/filaments thus reducing the network connectivity, resulting in a larger mesh size.

In suspended cells, however, we find the mesh size is not significantly affected by latrunculin A. We suspect that since suspended cells originally have a thicker cortex with more actin than adhered cell, even with latrunculin A treatment the cortex remains thick
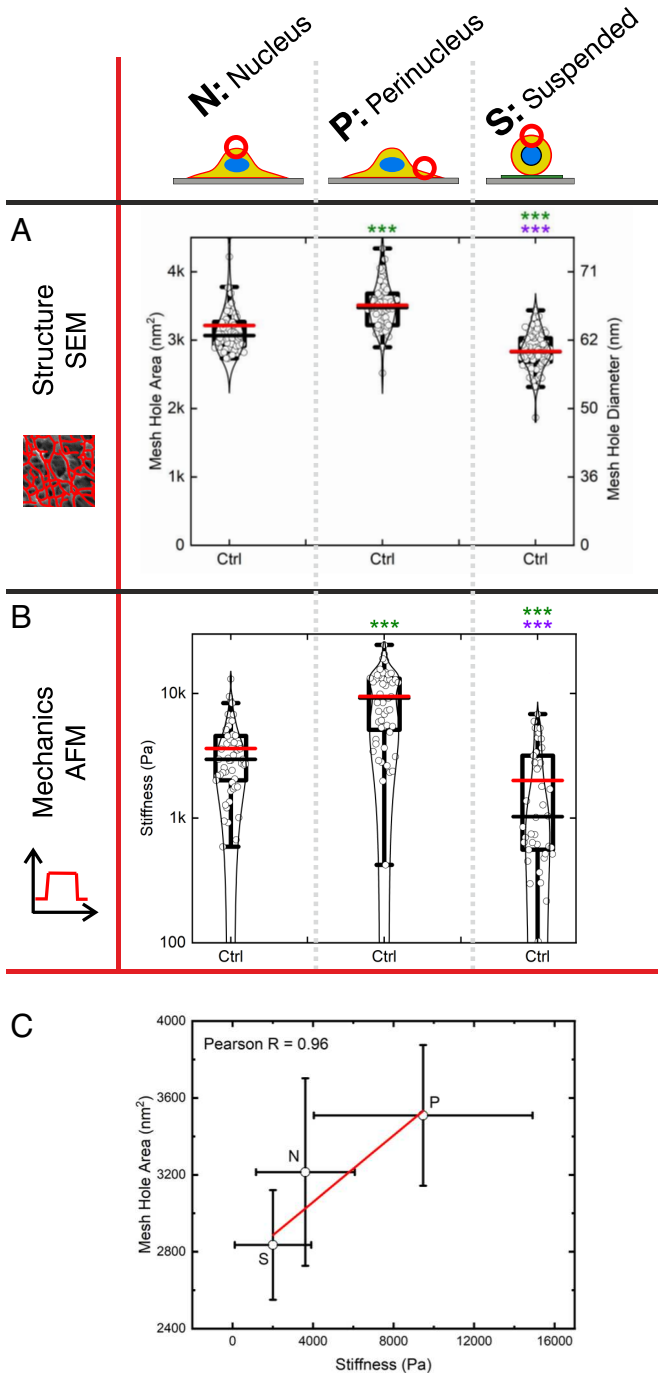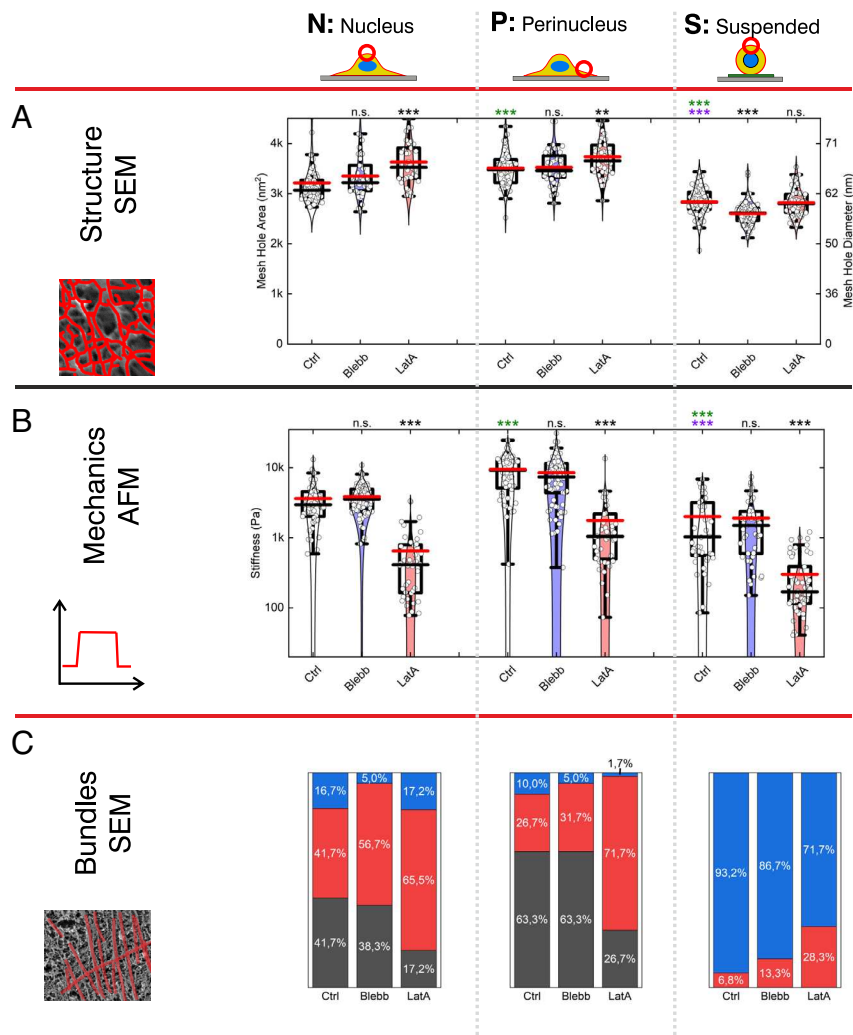
Fig. 4. Effect of blebbistatin and latrunculin A on structure and mechanics of the cellular cortex of adhered (nucleus and perinucleus) and suspended hTERT-RPE1 cells. (*A*)The mesh size of the actin cortex was quantitatively analyzed using SEM images using software FiNTA. (*B*) The stiffness was quantitatively analyzed employing creep compliance measurements using AFM. Stars represent statistical Welch-corrected *t* tests. Black stars compare treated cells with the controls for each panel, green stars compare controls to nucleus controls, and purple stars compare suspended controls to perinucleus controls. n.s.: not significant, *P < 0.05, **P < 0.01, ***P < 0.001. Cell numbers n are in the order controls, blebbistatin, latrunculin: Structure (SEM): nucleus: n = 63, 39, 37; perinucleus: n = 57, 40, 44; suspended cells: n = 66, 75, 61; Mechanics (AFM): nucleus: n = 53, 88, 40; perinucleus: n = 52, 73, 43; suspended cells: n = 42, 47, 54. (*C*) Bar charts of percentages of images showing many (black), few (red), or no (blue) bundles in SEM images (~30 images per region).

enough to prevent the loss of network connectivity thus keeping the small mesh size of the untreated cells but reducing the cortex thickness. It is worth noting that assuming actin filaments generally have their barbed (plus) ends pointing outward (48), depolymerization will occur generally from the inside, thus thinning the cortex before affecting the outer surface. Our SEM images confirm that at the latrunculin A concentration we use (0.1 mM), the outer surface of the cortex remains intact (*SI Appendix*, Fig. SI9*A*). However, larger concentrations of latrunculin A can break up the cortex as seen in (*SI Appendix*, Fig. SI9*B*).

Stiffness decreases with latrunculin A treatment in all cells (Fig. 4*B*). This is expected due to the decrease in actin concentration (46, 49) and the strong dependence of biopolymer network stiffness on actin concentration shown in Eq. **2** (15) and was previously observed by others (50). Physically, the increased mesh size in adhered cells results in a softer network. In suspended cells, the thinner cortex is softer since it can bend more easily.

It is noteworthy that in adhered cells treated with latrunculin A, we see a negative correlation between mesh size and stiffness. This is contrary to what we saw when comparing untreated

adhered cells with untreated suspended cells in which the correlation was positive. These two opposite correlation behaviors are seen depending on whether actin concentration is held constant with bundling changing as seen in Figs. 2*G* and 3 (positive correlation) or bundling held constant while actin concentration changes as seen in Fig. 4 *B* and *D* (negative correlation).

Discussion and Conclusion

We have shown and quantitatively described how the structure and mechanics of the actin cortex differ when cells are suspended compared to when they are adhered. We find that changes in the mesh size and stiffness between different cortex regions are positively correlated. We established a protocol to measure the thickness of the actin cortex in adhered cells using expansion microscopy. Using this technique, we find there is a similar amount of actin in the nuclear and perinuclear regions of adhered cells. In contrast, we see more actin in the cortex of suspended cells compared to adhered cells but less actin bundling.

A Microscopic Model of Actin Cortex Structure Predicts Mechanical Stiffness in Living Cells. The scheme (Fig. 5) shows our understanding of the relationship between mesh size and stiffness in the cell cortex. If the amount of actin increases without increased cross-linking (Fig. 5A) the mesh size decreases and the network becomes stiffer, i.e., a negative correlation between mesh size and stiffness. This is the same as seen in the in vitro work of ref. 14 on changing the actin concentration keeping cross-linking constant. We see this effect at work in our data with latrunculin A treatment on adhered cells, which results in a larger mesh size and softer network. If the amount of actin remains the same but there is an increase in proteins that cause bundling, the mesh size increases (Fig. 5B). In this case, the mesh becomes stiffer due to the bundles being stiffer than single filaments. This results in a positive correlation between increased mesh size and increased stiffness, as seen in ref. 14. We see this effect in our adhered cells since we see evidence of increased bundling in the stiffer perinuclear region compared to the softer nuclear region. We suggest this bundling is not caused by myosin II but by another actin bundling protein or by strain alignment of actin filaments, because inhibition of myosin II activity did not significantly change mesh size and stiffness in adhered cells. However, myosin has multiple effects (Fig. 5 C–F) as discussed later.

We summarize our findings by mapping them onto a theoretical map (Fig. 5G). This is a contour plot of the mesh size and stiffness on a graph with bundling on the vertical axis against actin concentration on the horizontal axis. The stiffness is given by Eq. **2** which comes from MacKintosh's polymer theory (15). The mesh size is given by Eq. **4** which comes from ref. 14.

The left-hand side of the theoretical map (Fig. 5G), corresponding to low actin concentrations, shows a large mesh size and low stiffness. The top right (high actin concentration and high bundling) is stiff for a variety of mesh sizes from medium to small for the highest actin concentration. We can map the cell adhesion states we have studied onto this diagram. Adhered cells are positioned in the middle of the diagram. Suspended cells have more actin in the cortex and less bundling than adhered cells and are in the region with small mesh size and relatively soft network.

We can also visualize the effects of latrunculin A treatment on this theoretical diagram by moving horizontally left to lower actin concentrations. We see that for adhered cells, the mesh size increases. This is also the case for suspended cells but more gradually and therefore moving a small distance may not show a significant effect. Moving horizontally left to lower actin concentrations also moves away from the stiff region to softer, as seen in our experiments.

Therefore, we show that the bundled biopolymer theory by MacKintosh al. (15) holds in living cells despite the cortex being more complex than the bundled actin system assumed in the theory and measured in vitro.
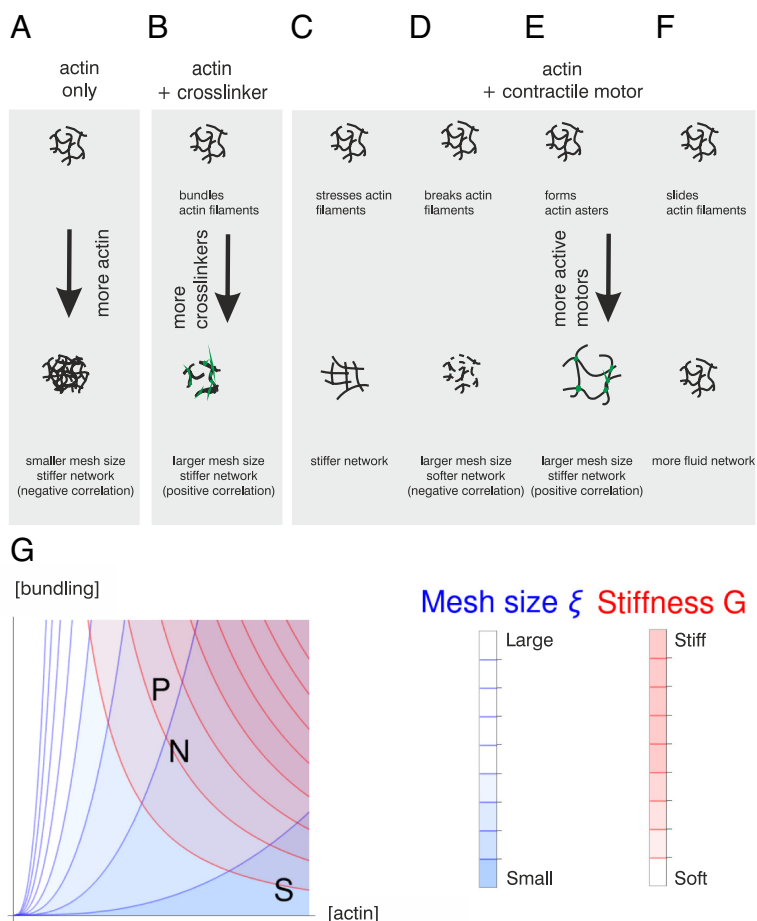

Fig. 5. Conceptual overview. (A–F) Scheme of effects of actin concentration, actin cross-linker, and actin cross-linker plus contractile motors on the actin mesh. (G) Theoretical map. Contour plot of mesh size given by Eq. **4**, $\xi = [bundling]^{0.3}/[actin]^{0.8}$ with the color scale blue–white corresponding to small–large mesh size.

Contour plot of stiffness given by G $= [actin]^{2.5} \left([bundling]^{0.3}/[actin]^{0.3} \right)^3$ with the color scale white-red corresponding to soft-stiff. White regions are soft with large mesh size, and purple regions are stiff with small mesh size. The cases measured here are plotted in: P stands for adhered cell, perinuclear region, N stands for adhered cell, nuclear region, S stands for suspended cell.

The Multifaceted Role of Myosin on Structure and Mechanics in Living Cells Remains an Open Question for the Field. As detailed in section *SI Appendix, Myosin* while we do not think myosin is responsible for the actin bundling, we see, we do observe myosin affecting the actin network in suspended cells (*SI Appendix, Cortex Thickness and Mesh Size*). Actomyosin is a more complex system than that assumed by MacKintosh et al. in the polymer theory and in the in vitro experiments with actin and the nonmotor cross-linker scruin performed by Gardel et al. and Shin et al. (14, 29). Gardel et al. (51) show that the effects of myosin activity depend on the architecture of actin bundles.

In our cells, we expect myosin to have multiple effects. In the following, we summarize different effects myosin may have. Actomyosin contractility can stiffen the network by exerting pre-stress on the network (Fig. 5C) (10, 52). In extreme cases, myosin activity can result in the breakage of actin filaments and network disassembly (53, 54), which in turn would lead to a larger mesh size and softer network similar to what is seen with decreasing actin concentration (Fig. 5D).

Clusters of myosin can also change the structure of the actin by forming asters of actin (Fig. 5E). This is seen in vitro by Vogel et al. (55, 56) and in cells by Verkhovsky et al. (57). This mechanism also increases the mesh size but without increasing bundling. We expect this clustering to also increase the stiffness since actin asters are likely to be stiffer than single actin filaments as seen by Murrell and Gardel (58). In this case, the mesh size and stiffness are positively correlated. We see such myosin clusters in suspended cells (*SI Appendix*, Fig. SI10) which have more actin, a smaller mesh size, less bundling, and are softer. The suspended cells have more myosin clusters in the cortex than adhered cells. We might expect such myosin clusters and actin asters to increase the mesh size and stiffen the network, however, in our suspended cells we see a smaller mesh size and softer network corresponding with more actin and less bundling. Similarly, it was previously shown that when Vero cells detach from the substrate, a notable decrease in Young's modulus was observed, however it appeared to correlate with the disassembly of stress fibers (59).

If our expectation that active myosin does increase the mesh size is correct, we would see a decrease in mesh size on inactivating myosin. We tested this using blebbistatin treatment in suspended cells and indeed observed a decrease in mesh size (Fig. 4A).

There is a final way in which myosin can act, namely its motor activity sliding filaments along each other and thus decreasing the stiffness (60) (Fig. 5F). This mechanism is likely to occur in suspended cells due to less anchoring of the actin cortex to the surrounding, partly explaining why their cortex is softer despite the increased amount of myosin compared to adhered cells. We expect the reduction in myosin activity caused by blebbistatin to increase the stiffness compared to the softened active network. However, the effect described in Fig. 5E would decrease the stiffness due to the reduction in myosin cluster forming asters. In fact, we see no significant difference in the stiffness with blebbistatin treatment in suspended cells (Fig. 4B), indicating that these opposing effects are compensatory.

Mesh Size and Stiffness of the Cortex Depend on the Cell State. In conclusion, we showed how the mesh size and stiffness of the cortex differ depending on whether a cell is adhered or suspended. In particular, we measured the cortex thickness in adhered as well as in suspended cells. We used FiNTA to measure the cortical mesh size in SEM images. Characterizing the structure and mechanics of the cortex in different situations is essential in explaining various cell properties from morphology to migration behavior. In turn, the effects of these in living organisms are crucial to the progression of health and disease. In this work, we characterized the differences in properties of the cortex between two states of cells, namely adhered and suspended. We can view these as particular points in a state space and consider transitions between them. In the future, it will be possible to characterize other points within state space, for example cells with/without confinement. Due to the complex nature of cellular materials, corresponding state spaces are multidimensional. Here, we consider the key parameters of the structure and mechanics of the cortex (mesh size, stiffness, and bundling). We show that both mesh size and bundling play an equally important role in this phase space, however, with means of today the mesh size is still easier to obtain. Future will provide better tools to quantitatively assess the bundling of actin in the cortex. In addition, there are other parameters that might be important to characterize state transitions within multidimensional phase spaces. For example, it was shown that the process of cell spreading requires a temporary reduction in cortical tension, facilitating the formation of membrane protrusions. These protrusions, in turn, enable the cell to expand and spread (61). More work is required to establish which parameters define which transitions. In this work, we provide a starting point by mapping the important properties of the actin cortex and how it differs between two cell states that are key to function.

Author affiliations: ªDepartment of Physics, Saarland University, Saarbrücken 66123, Germany; ᵇFaculty of Science, Institute of Applied Physics, University of Tübingen, Tübingen 72076, Germany; ᶜDepartment of Biophysical Chemistry, Georg-August-University, Göttingen 37077, Germany; ᵈCenter for Genomic Regulation (CRG), The Barcelona Institute of Science and Technology, Barcelona 08003, Spain; ᵉUniversitat Pompeu Fabra, Barcelona 08002, Spain; ᶠInstitució Catalana de Recerca i Estudis Avançats (ICREA), Barcelona 08010, Spain; ᵍDepartment of Physics and Astronomy, University of Sheffield, Sheffield S3 7RH, United Kingdom; ʰAfrican Institute for Mathematical Sciences, Accra 20046, Ghana; and ⁱCenter for Biophysics, Saarland University, Saarbrücken 66123, Germany

1. P. Chugh, E. K. Paluch, The actin cortex at a glance. *J. Cell Sci.* **131**, jcs186254 (2018).
2. D. A. Fletcher, R. D. Mullins, Cell mechanics and the cytoskeleton. *Nature* **463**, 485–492 (2010).
3. G. Salbreux, G. Charras, E. Paluch, Actin cortex mechanics and cellular morphogenesis. *Trends Cell Biol.* **22**, 536–545 (2012).
4. T. D. Pollard, Actin and actin-binding proteins. *Cold Spring Harb. Perspect. Biol.* **8**, a018226 (2016).
5. T. D. Pollard, L. Blanchoin, R. D. Mullins, Molecular mechanisms controlling actin filament dynamics in nonmuscle cells. *Annu. Rev. Biophys.* **29**, 545–576 (2000).
6. N. Castaneda, J. Park, E. H. Kang, Regulation of actin bundle mechanics and structure by intracellular environmental factors. *Front. Phys.* **9**, 675885 (2021).
7. P. Matsudalra, Modular organization of actin crosslinking proteins. *Trends Biochem. Sci.* **16**, 87–92 (1991).
8. M. Schliwa, G. Woehlke, Molecular motors. *Nature* **422**, 759–765 (2003).
9. F. Lautenschläger et al., The regulatory role of cell mechanics for migration of differentiating myeloid cells. *Proc. Natl. Acad. Sci. U.S.A.* **106**, 15696–15701 (2009).
10. A. Cordes et al., Prestress and area compressibility of actin cortices determine the viscoelastic response of living cells. *Phys. Rev. Lett.* **125**, 068101 (2020).
11. C. J. Chan et al., Myosin II activity softens cells in suspension. *Biophys. J.* **108**, 1856–1869 (2015).
12. D. Bray, J. G. White, Cortical flow in animal cells. *Science* **239**, 883–888 (1988).

13. S. Mukhina, Y. Wang, M. Murata-Hori, α-actinin is required for tightly regulated remodeling of the actin cortical network during cytokinesis. *Dev. Cell* **13**, 554–565 (2007).
14. M. L. Gardel *et al.*, Elastic behavior of cross-linked and bundled actin networks. *Science* **304**, 1301–1305 (2004).
15. F. C. MacKintosh, J. Käs, P. A. Janmey, Elasticity of semiflexible biopolymer networks. *Phys. Rev. Lett.* **75**, 4425–4428 (1995).
16. A. Colin, P. Singaravelu, M. Théry, L. Blanchoin, Actin-network architecture regulates microtubule dynamics. *Curr. Biol.* **28**, 2647–2656 (2018).
17. J. Azoury *et al.*, Spindle positioning in mouse oocytes relies on a dynamic meshwork of actin filaments. *Curr. Biol.* **18**, 1514–1519 (2008).
18. S. J. Winder, K. R. Ayscough, Actin-binding proteins. *J. Cell Sci.* **118**, 651–654 (2005).
19. M. Schnoor, Endothelial actin-binding proteins and actin dynamics in leukocyte transendothelial migration. *J. Immnuol.* **194**, 3535–3541 (2015).
20. T. A. Springer, Traffic signals on endothelium for lymphocyte recirculation and leukocyte emigration. *Ann. Rev. Physiol.* **57**, 827–872 (1995).
21. R. A. Whipple, A. M. Cheung, S. S. Martin, Detyrosinated microtubule protrusions in suspended mammary epithelial cells promote reattachment. *Exp. Cell Res.* **313**, 1326–1336 (2007).
22. M. Schu *et al.*, Scanning electron microscopy preparation of the cellular actin cortex: A quantitative comparison between critical point drying and hexamethyldisilazane drying. *PLoS One* **16**, e0254165 (2021).
23. D. A. D. Flormann *et al.*, Oscillatory microrheology, creep compliance and stress relaxation of biological cells reveal strong correlations as probed by atomic force microscopy. *Front. Phys.* **9**, 71186 (2021).
24. P. Chugh *et al.*, Actin cortex architecture regulates cell surface tension. *Nat. Cell Biol.* **19**, 689–697 (2017).
25. V. Laplaud *et al.*, Pinching the cortex of live cells reveals thickness instabilities caused by myosin II motors. *Sci. Adv.* **7**, eabe3640 (2021).
26. C. A. Combs, H. Shroff, Fluorescence microscopy: A concise guide to current imaging methods. *Curr. Protoc. Neurosci.* **79**, 2.1.1–2.1.25 (2017).
27. F. Chen, P. W. Tillberg, E. S. Boyden, Optical imaging. Expansion microscopy. *Science* **347**, 543–548 (2015).
28. A. G. Clark, K. Dierkes, E. K. Paluch, Monitoring actin cortex thickness in live cells. *Biophys. J.* **105**, 570–580 (2013).
29. J. H. Shin, M. L. Gardel, L. Mahadevan, P. Matsudaira, D. A. Weitz, Relating microstructure to rheology of a bundled and cross-linked F-actin network in vitro. *Proc. Natl. Acad. Sci. U.S.A.* **101**, 9636–9641 (2004).
30. D. A. D. Flormann *et al.*, A novel universal algorithm for filament network tracing and cytoskeleton analysis. *FASEB J.* **35**, e21582 (2021).
31. L. Hauke *et al.*, FilamentSensor 2.0: An open-source modular toolbox for 2D/3D cytoskeletal filament tracking. *PLoS One* **18**, e0279336 (2023).
32. J. Schindelin *et al.*, Fiji: An open-source platform for biological-image analysis. *Nat. Methods* **9**, 676–682 (2012).
33. J. Kolega, Cytoplasmic dynamics of myosin IIA and IIB: Spatial sorting of isoforms in locomoting cells. *J. Cell Sci.* **111**, 2085–2095 (1998).
34. J. X. Tang, T. Ito, T. Tao, P. Traub, P. A. Janmey, Opposite effects of elecrostatics and steric exclusion on bundle formation by F-Actin and other filamentous polyelectrolytes. *Biochemistry* **36**, 12395–12652 (1997).
35. J. Schnauß, T. Händler, J. A. Käs, Semiflexible biopolymers in bundled arrangements. *Polymers (Basel)* **8**, 274 (2016).
36. M. Hosek, J. X. Tang, Polymer-induced bundling of F actin and the depletion force. *Phys. Rev. E Stat. Nonlin. Soft Matter Phys.* **69**, 051907 (2004).
37. A. M. Greiner, H. Chen, J. P. Spatz, R. Kemkemer, Cyclic tensile strain controls cell shape and directs actin stress fiber formation and focal adhesion alignment in spreading cells. *PLoS One* **8**, e77328 (2013).
38. D. R. Scheff *et al.*, Actin filament alignment causes mechanical hysteresis in cross-linked networks. *Soft Matter* **17**, 5499–5507 (2021).
39. K. M. Schmoller, P. Fernández, R. C. Arevalo, D. L. Blair, A. R. Bausch, Cyclic hardening in bundled actin networks. *Nat. Commun.* **1**, 134 (2010).
40. G. Žagar, Patrick R. Onck, E. van der Giessen, Two fundamental mechanisms govern the stiffening of cross-linked networks. *Biophys. J.* **108**, 1470–1479 (2015).
41. C. Storm, J. J. Pastore, F. C. MacKintosh, T. C. Lubensky, P. A. Janmey, Nonlinear elasticity in biological gels. *Nature* **435**, 191–194 (2005).
42. D. A. D. Flormann *et al.*, The role of actin and myosin II in the cell cortex of adhered and suspended cells. bioRxiv [Preprint] (2021). https://doi.org/10.1101/2021.08.03.454901 (Accessed 4 August 2021).
43. B. Fabry *et al.*, Scaling the microrheology of living cells. *Phys. Rev. Lett.* **87**, 148102 (2001).
44. F. M. Hecht *et al.*, Imaging viscoelastic properties of live cells by AFM: Power-law rheology on the nanoscale. *Soft Matter* **11**, 4584–4591 (2015).
45. M. Kovács, J. Tóth, C. Hetényi, A. Málnási-Csizmadia, J. R. Sellers, Mechanism of blebbistatin inhibition of myosin II. *J. Biol. Chem.* **279**, 35557–35563 (2004).
46. M. Coué, S. L. Brenner, I. Spector, E. D. Korn, Inhibition of actin polymerization by latrunculin A. *FEBS Lett.* **213**, 316–318 (1987).
47. A. X. Cartagena-Rivera, J. S. Logue, C. M. Waterman, R. S. Chadwick, Actomyosin cortical mechanical properties in nonadherent cells determined by atomic force microscopy. *Biophys. J.* **110**, 2528–2539 (2016).
48. T. Svitkina, The actin cytoskeleton and actin-based motility. *Cold Spring Harb. Perspect. Biol.* **10**, a018267 (2018).
49. W. M. Morton, K. R. Ayscough, P. J. McLaughlin, Latrunculin alters the actin-monomer subunit interface to prevent polymerization. *Nat. Cell Biol.* **2**, 376–378 (2000).
50. T. Wakatsuki, B. Schwab, N. C. Thompson, E. L. Elson, Effects of cytochalasin D and latrunculin B on mechanical properties of cells. *J. Cell Sci.* **114**, 1025–1036 (2001).
51. K. L. Weirich, S. Stam, E. Munro, M. L. Gardel, Actin bundle architecture and mechanics regulate myosin II force generation. *Biophys. J.* **120**, 1957–1970 (2021).
52. D. Mizuno, C. Tardin, C. F. Schmidt, F. C. MacKintosh, Nonequilibrium mechanics of active cytoskeletal networks. *Science* **315**, 370–373 (2007).
53. C. A. Wilson *et al.*, Myosin II contributes to cell-scale actin network treadmilling through network disassembly. *Nature* **465**, 373–377 (2010).
54. M. P. Murrell, M. L. Gardel, F-actin buckling coordinates contractility and severing in a biomimetic actomyosin cortex. *Proc. Natl. Acad. Sci. U.S.A.* **109**, 20820–20825 (2012).
55. S. K. Vogel, Z. Petrasek, F. Heinemann, P. Schwille, Myosin motors fragment and compact membrane-bound actin filaments. *Elife* **2**, e00116 (2013).
56. S. Stam *et al.*, Filament rigidity and connectivity tune the deformation modes of active biopolymer networks. *Proc. Natl. Acad. Sci. U.S.A.* **114**, E10037–E10045 (2017).
57. A. B. Verkhovsky, T. M. Svitkina, G. G. Borisy, Polarity sorting of actin filaments in cytochalasin-treated fibroblasts. *J. Cell Sci.* **110**, 1693–1704 (1997).
58. M. Murrell, M. L. Gardel, Actomyosin sliding is attenuated in contractile biomimetic cortices. *Mol. Biol. Cell* **25**, 1845–1853 (2014).
59. Y. M. Efremov *et al.*, Distinct impact of targeted actin cytoskeleton reorganization on mechanical properties of normal and malignant cells. *Biochim. Biophys. Acta* 1853, 3117–3125 (2015).
60. D. Humphrey, C. Duggan, D. Saha, D. Smith, J. Käs, Active fluidization of polymer network through molecular motors. *Nature* **416**, 413–416 (2002).
61. A. Pietuch, A. Janshoff, Mechanics of spreading cells probed by atomic force microscopy. *Open Biol.* **3**, 130084 (2013).
62. F. Lautenschläger, D. A. D. Flormann, Data for Manuscript: The structure and mechanics of the cell cortex depends on location and adhesion state. Figshare. Dataset. https://doi.org/10.6084/m9.figshare.26139370.v1. Deposited 1 July 2024.